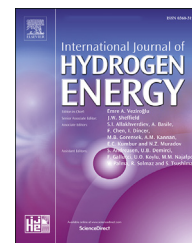




ELSEVIER

Available online at www.sciencedirect.com

ScienceDirect

journal homepage: www.elsevier.com/locate/he

Modeling a hydrogen pressure regulator in a fuel cell system with Joule–Thomson effect

Jixin Chen ^{a,*}, Mike Veenstra ^a, Justin Purewal ^a, Bert Hobein ^b,
Stella Papasavva ^a

^a Ford Motor Company, Dearborn, MI, 48121, USA

^b Ford-Werke GmbH, Aachen, 52072, Germany

ARTICLE INFO

Article history:

Received 22 June 2018

Received in revised form

25 October 2018

Accepted 1 November 2018

Available online xxx

Keywords:

Pressure regulator

Joule–Thomson effect

Hydrogen tank

Fuel cell vehicle

ABSTRACT

Fuel cell vehicles offer significant sustainability benefits by eliminating tailpipe emissions, increasing powertrain efficiency, and utilizing hydrogen that can be supplied from various sources including renewables. A pressure regulator in the hydrogen storage system on a fuel cell vehicle is an important component to ensure that the hydrogen delivery to the fuel cell stack meets the pressure and temperature requirements. A validated model of the regulator can be used to support the product design and optimization of the operating strategy. In this work, a pressure regulator model has been developed to capture the hydrogen discharge behaviors from the compressed hydrogen tank to the fuel cell stack. The focus of the model is to develop the pressure and temperature relationship at the regulator outlet given the inlet conditions from the storage tank. Besides the ideal-gas based derivation for pressure response, the model has used a constant-enthalpy approach to capture the hydrogen temperature increase associated with the pressure drop due to the Joule–Thomson effect. The model was validated with various testing data including hysteresis and dynamic flow conditions, showing satisfactory agreement. The validated model was then used for parametric studies. The modeling results concluded that the regulator inlet temperature has the strongest influence on raising the outlet temperature, while the regulator inlet pressure is an important factor although secondary to the inlet temperature. The comprehensive regulator modeling developed in this work provides the foundation for assessing and optimizing a key dynamic component in the hydrogen storage system.

© 2018 Hydrogen Energy Publications LLC. Published by Elsevier Ltd. All rights reserved.

Introduction

A fuel cell vehicle is regarded as an important zero-emission alternative that features comparable driving range and refilling time with internal-combustion-engine vehicles [1]. There are many model-based studies to improve the fuel cell system and control in a vehicular application [2–6]. Bao et al. [2,3] developed a dynamic model of fuel cell system to control

and optimize the transient behaviors of air supply and hydrogen recirculation considering the mixed effects of gas flow, pressure and humidity. Hatti and Tioursi [4] demonstrated an artificial intelligence technique to control a proton exchange membrane fuel cell system process using a dynamic neural network. The anode recirculation system has been studied with theoretical modeling by Dadvar and Afshari [5], focusing on the optimization of stack and ejector design parameters. The pressure control components play an

* Corresponding author.

E-mail address: jchen186@ford.com (J. Chen).

<https://doi.org/10.1016/j.ijhydene.2018.11.020>

0360-3199/© 2018 Hydrogen Energy Publications LLC. Published by Elsevier Ltd. All rights reserved.

important role for the desired system performance. Hong et al. [6] presented a control oriented dynamic model for the fuel delivery system with anode recirculation and anode bleeding. Based on the model, a multi-input-multi-output nonlinear state feedback controller along with an optimized output feedback controller is proposed to maintain adequate hydrogen supply and suitable anode hydrogen concentration.

However, as a typical simplification, an ideal behavior of reaching desired pressure from hydrogen tank without fluctuation and delay was assumed in these studies. Realistically, the dynamic response of pressure regulators and valves upon load change could influence the performance of system components and stack. For example, the primary flow rate as well as the recirculation ratio of an anode ejector is dependent on the upstream pressure [7]. Insufficient hydrogen supply upon load change could also lead to anode reversal and durability concern such as carbon corrosion [8], besides impacting the stack performance [9] and the accuracy of the abovementioned control strategies. Some component optimization for anode pressure management has been performed. For example, Chen et al. [10] proposed a two-step high pressure reducing system for fuel cell vehicle comprised of a high multi-stage pressure reducing valve and a multi-stage muffler. Flow field, energy consumption and thermal-mechanical stress were investigated for the robustness of the proposed system. Hu et al. [11] found that a greater diameter of purge valve can lead to a better stack performance as well as voltage stability during a dead-ended anode operation.

Therefore, it is important to examine the system components involved with hydrogen supply. On a fuel cell vehicle, the key components of the hydrogen storage system consist of compressed hydrogen tank(s), on-tank valve(s), and pressure regulator(s) [12,13]. During vehicle operation, the regulator reduces the high pressure from the tank and delivers the hydrogen to the fuel cell system within a limited pressure tolerance to sustain the fuel cell performance. The challenge for the pressure regulator is to maintain an outlet pressure within a narrow tolerance of only a couple bars despite fluctuations in the flow rate, inlet pressure, and gas temperatures. In addition, the regulator has limits on the outlet hydrogen temperature for the operation of the downstream fuel cell stack. A regulator consists of three functional elements: a pressure reducing or restrictive element, often a spring loaded poppet valve; a sensing element, typically a diaphragm or piston; and a reference force element, most commonly a spring. In operation, the reference force generated by the spring opens the valve. The opening of the valve applies pressure to the sensing element which in turn closes the valve until it is open just enough to maintain the set pressure [14].

Despite its important role to ensure an effective control of the fuel cell system, there is limited analytical work on the pressure regulator in the literature. A dome-loaded pressure regulator has been modeled by Nabi et al. [15] With this model, ideal-gas based thermodynamic analysis was conducted to calculate the air pressure at the outlet with comparison against data in initial transient (<0.5 s) of pressure step change. However, the pressure validation in a longer period was not reported. Rami et al. [16] developed a 1st principle based pressure regulating station model which includes a regulator, a shut-off valve, a meter and pipelines, which was used for natural gas

delivery. Zafer and Luecke [17] developed a pressure regulator model to investigate the stability characteristics of the regulator components and the resulted outlet pressure fluctuation. Using root locus techniques, the design parameters were optimized to reduce such vibration. Sun et al. [18] modeled a typical pressurized system with a novel dual-stage gas pressure reducing regulator in an aerospace flight application, and demonstrated an excellent dynamic behaviors of the pressure reducing regulator. Since these previous models were not for vehicle dynamic applications, the temperature response in dynamic conditions was not a particular focus, which resulted in ideal-gas equations being used to calculate temperature from pressure. The temperature response during hydrogen tank filling has been modeled with non-ideal-gas equations [19,20] showing improved prediction than ideal-gas based models. However, the tank filling is a different phenomenon than the pressure release through the regulator. Also, the mathematical derivation in these approaches [19,20] could be simplified for an actual implementation of the model.

For a real gas, as differentiated from an ideal gas, the Joule–Thomson effect refers to the temperature change when a gas is throttled through a valve or orifice without heat exchanged with the environment due to sufficiently fast flow. In literature, there are analytical and experimental studies [21–25] on the gas temperature and pressure during a tank refilling for a fuel cell vehicle which involves the Joule–Thomson effect of hydrogen. Hydrogen has a negative Joule–Thomson coefficient leading to an increased temperature with pressure reduction, which could be a practical concern for refilling a fuel cell vehicle. Depending on the refilling conditions, the Joule–Thomson effect may contribute insignificantly to the gas temperature increase as compared to the compression of the gas in the tank due to the incoming high pressure and the conversion of kinetic energy into internal energy [22,24,25]. In another application, Joule–Thomson effect caused significant temperature increase and became an important consideration in designing precooling units at hydrogen refueling stations [26]. For a regulator which delivers hydrogen from the tank to the fuel cell stack, it is also important to capture the temperature response associated with the pressure change from Joule–Thomson effect. In some tests, it is observed that the hydrogen gas temperature at regulator outlet reached 115°C due to the high flow demand as shown in Fig. 1. The increase in temperature can be an issue for the robustness of materials within the regulator and fuel cell. The specified limit for the hydrogen gas temperature for the regulator and fuel cell is 85°C . The capability with the model to predict the gas temperature dynamics at the outlet pressure side of the regulator is essential to ensure that the operation remains within the temperature limit.

In this work, it is aimed to develop a physics-based pressure regulator model to simulate the H_2 delivery performance required for an automotive fuel cell system. The objective of the model is to calculate the transient pressure and temperature at the outlet of the regulator given the required flow rate and inlet conditions. The Joule–Thomson effect induced temperature increase is captured in the model through a constant-enthalpy approach, which was shown to provide better utility and implementation than the derivation of thermodynamic equations [19,20]. The model is validated

using the data from system bench tests that simulate the anode supply line of a fuel cell system. The model outcome is a virtual regulator with the functional transfer functions to evaluate and benchmark designs to reduce the actual testing. In the following section, the model assumptions and equations are discussed. The model has been used to produce simulation results for both hysteresis and dynamic flow conditions. The validation with various dynamic conditions, which has not been done for previous regulator models in literature, will be shown to demonstrate the robustness of the model. Finally parametric studies are performed using the validated model.

Model development

Fig. 2 is a schematic showing the regulator structure in the model. The key component in the regulator is the piston that is in contact with two spring forces. The piston moves based on the net force applied which results in varying the size of the orifice opening. When the piston moves towards the left in Fig. 2 due to increased pressure in the downstream volume, the orifice opening is reduced resulting in a restricted flow rate across the orifice. When the piston moves to the right, the orifice opens and the flow rate across the orifice increases. This feedback mechanism ensures accurate pressure regulation based on the downstream pressure. The desired set point of the outlet pressure is determined by the force balance and preloading from two springs.

When flow is introduced as indicated by the red arrow, it passes through the orifice and increases pressure in the low-pressure volume (V_L). Such increasing pressure applies a force moving the piston towards the left in Fig. 2. If such a force overcomes the preloading and generates a net force moving the piston towards the left, then the orifice size is reduced which prevents the pressure in the low-pressure volume from further increase. In the event of decreasing pressure in the low-pressure volume due to hydrogen supply

to the fuel cell, a net force will move the piston towards the right and the orifice size enlarges for increased flow. Therefore, the piston adjusts its position until an equilibrium is reached, which corresponds to the preset pressure at the low-pressure volume.

Model equations

As shown in Fig. 3, the model is constructed by connecting a few ideal-gas based control-volume equations corresponding to the physical volumes from the regulator to the downstream pressure transducer. V_H represents the total volume prior to the orifice including the pipeline volume from the tank to the regulator. V_L is the volume from the orifice to the outlet of the regulator, and V_{tr} is the volume from the outlet to the pressure transducer whose data are used for model validation in the next section.

The conservation of momentum equation (Eq. (1)) was used to describe the motion of piston. The right-hand-side (RHS) of Eq. (1) are the forces on the piston including a preloaded spring force, spring force due to the piston moving away from its original position, mechanical friction, and various pressures on the corresponding surfaces of the piston.

$$M\ddot{x} = F_s - kx - f \cdot \text{sgn}(\dot{x}) - \sum A_i P_i \quad (1)$$

A control volume function for an open system will yield the following:

$$\frac{dE_{CV}}{dt} = \dot{m}_{in} h_{in} - \dot{m}_{out} h_{out} \quad (2)$$

where h is the specific enthalpy of the gas, and E is the internal energy. The left-hand-side (LHS) of Eq. (2) can be written as:

$$\begin{aligned} LHS &= \frac{d(mc_v T)}{dt} = c_v T_{out} \frac{dm}{dt} + c_v m \frac{dT_{out}}{dt} \\ &= c_v T_{out} (\dot{m}_{in} - \dot{m}_{out}) + c_v \frac{PVM}{RT_{out}} \frac{dT_{out}}{dt} \end{aligned} \quad (3)$$

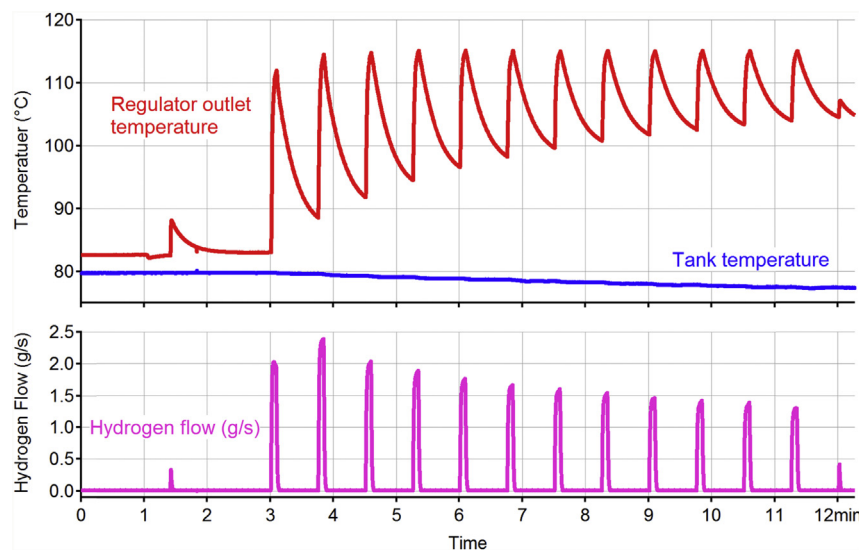


Fig. 1 – Regulator test data demonstrating high outlet temperatures due to the Joule–Thomson effect.

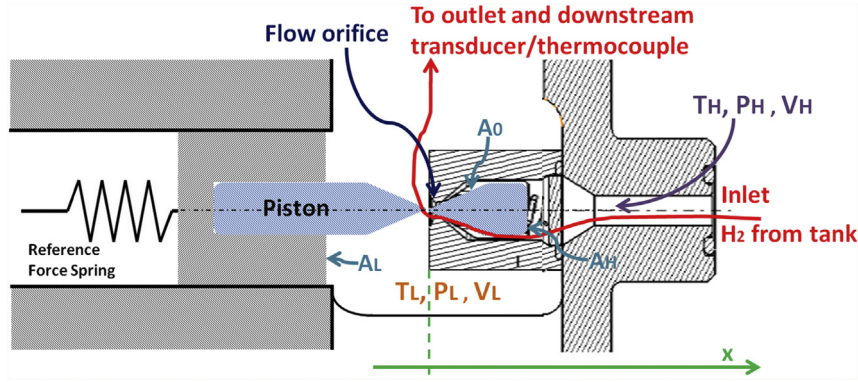


Fig. 2 – The structure of the regulator being modeled. Hydrogen passes through a pressure restrictive element connecting high-pressure and low-pressure volumes of the regulator to arrive the downstream tubing and sensors.

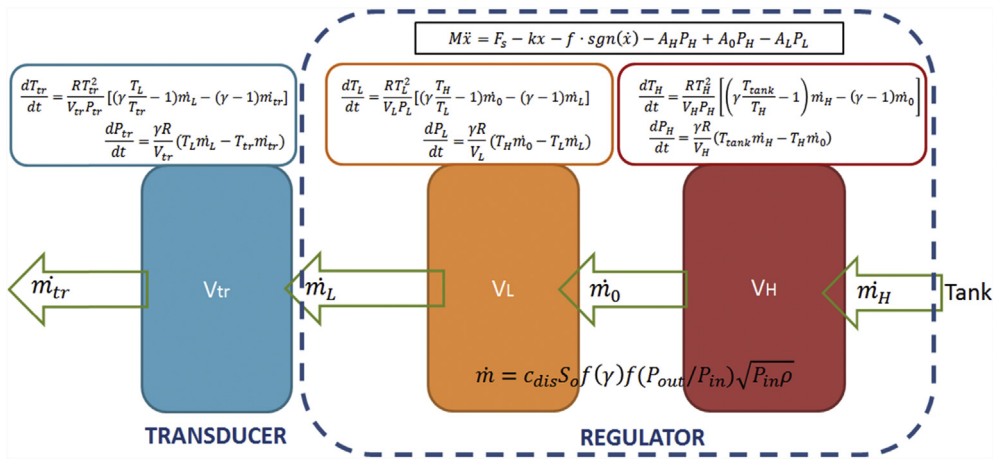


Fig. 3 – The modeling domain and equations.

Equating with the RHS of Eq. (2) and using $h = c_p T$ yields:

$$c_v T_{out} (\dot{m}_{in} - \dot{m}_{out}) + c_v \frac{PVM}{RT_{out}} \frac{dT_{out}}{dt} = \dot{m}_{in} c_p T_{in} - \dot{m}_{out} c_p T_{out} \quad (4)$$

After rearrangement the following equation can be obtained:

$$\frac{dT_{out}}{dt} = \frac{RT_{out}^2}{PV} \left[\left(\gamma \frac{T_{in}}{T_{out}} - 1 \right) \dot{m}_{in} - (\gamma - 1) \dot{m}_{out} \right] \quad (5)$$

Eq. (2) can be derived into another form. With the ideal gas law, the LHS can be also rearranged:

$$LHS = \frac{d(mc_v T)}{dt} = \frac{c_v d(\frac{PV}{R})}{dt} = \frac{c_v V}{R} \frac{dP}{dt} \quad (6)$$

Equating with the RHS of Eq. (2) and noting the pressure in the control volume (P) being identical to the pressure at the control volume outlet (P_{out}), the following equation can be obtained:

$$\frac{c_v V}{R} \frac{dP_{out}}{dt} = \dot{m}_{in} c_p T_{in} - \dot{m}_{out} c_p T_{out} \quad (7)$$

which can be further rearranged with $\gamma = \frac{c_p}{c_v}$:

$$\frac{dP_{out}}{dt} = \frac{\gamma R}{V} \left(T_{in} \dot{m}_{in} - T_{out} \dot{m}_{out} \right) \quad (8)$$

The derived equations for pressure (Eq. (8)) and temperature (Eq. (5)) stem from the same ideal-gas based control volume analysis (Eq. (2)). Essentially, two unknown gas states (pressure and temperature) are solved from two equations (Eq. (2) and ideal-gas equation). Eqs. (2)–(8) are used for three continuous volumes in Fig. 3 (V_H , V_L , V_{tr}). The “in” and “out” subscripts have been replaced to denote each volume in Fig. 3.

The flow rate across each volume, i.e., the flow rate at the regulator inlet, variable-size orifice, and regulator outlet, can be calculated by [15]:

$$\dot{m} = c_{dis} S_o \left(\frac{2}{\gamma + 1} \right)^{\frac{1}{\gamma - 1}} \sqrt{\frac{2\gamma}{\gamma + 1} \frac{1}{RT_{hi}} P_{hi}} \quad \text{when } \frac{P_{lo}}{P_{hi}} < 0.528 \quad (9)$$

$$\dot{m} = c_{dis} S_o \sqrt{\frac{2\gamma}{\gamma - 1} \frac{1}{RT_{hi}} P_0} \sqrt{\left[\left(\frac{P_{lo}}{P_{hi}} \right)^{\frac{2}{\gamma}} - \left(\frac{P_{lo}}{P_{hi}} \right)^{\frac{\gamma + 1}{\gamma}} \right]} \quad \text{when } \frac{P_{lo}}{P_{hi}} \gg 0.528 \quad (10)$$

where C_{dis} is the discharge coefficient and is a tunable parameter in the model. S_0 is the size of the orifice or regulator inlet/outlet. The orifice size, $S_0(x)$, is a function of piston position based on the specific design from a spring force balance lookup table. P_{lo} and P_{hi} are the pressure at the low-pressure volume and high-pressure volume, respectively.

Eqs. (2)–(8) calculate gas pressure as well as temperature at each volume described in Fig. 3. The temperature calculation is coupled with pressure calculation in an ideal-gas framework assuming the gas is incompressible. Thus, the Joule–Thomson effect is not captured and the temperature calculation from these equations will be lower than reality, particularly if there is an abrupt increase of flow rate such as in Fig. 1. In the following, an equation has been further derived based on constant-enthalpy throughout the regulator for a stand-alone temperature sub-model. It should be noted that the pressure response is still calculated with an ideal-gas model frame as discussed above, which has shown satisfactory agreement with experimental data (see Model Validation section).

The enthalpy of gas at the inlet of the regulator is:

$$h_1 = P_{tank}V_1 - m c_p T_{tank} \quad (11)$$

where m is the mass of hydrogen that has been carried over through the regulator. The enthalpy of gas at the outlet of the regulator is:

$$h_2 = P_{tr}V_2 - m c_p T_2 \quad (12)$$

A compressibility factor Z [27] is considered in revising the ideal gas relationship:

$$mT_{tank} = \frac{P_{tank}V_1}{RZ(P, T)} \quad (13)$$

Due to the high pressure storage in the tank (700 bar), it is necessary to consider Z in Eq. (11) but not in Eq. (12) since Z is almost unity at low pressure. A lookup table is used to obtain Z value from pressure and temperature conditions [27]. Substituting Eq. (13) into Eq. (11) and Eq. (12) and assuming negligible heat transfer and friction due to a short residence time of the gas throughout the regulator, thereby equating the enthalpies at inlet (Eq. (11)) and outlet (Eq. (12)) yield:

$$P_{tr}V_2 - \frac{P_{tank}V_1}{T_{tank}RZ(P, T)}c_p T_2 = P_{tank}V_1 - \frac{P_{tank}V_1}{RZ(P, T)}c_p \quad (14)$$

After rearrangement, an algebraic equation for T_2 can be obtained:

$$T_2 = \frac{P_{tank}V_1 - P_{tr}V_2}{\frac{P_{tank}V_1 c_p}{RZ(P, T)T_{tank}}} + T_{tank} \quad (15)$$

where V_1 is the volume of tubing from the tank to the regulator inlet, and V_2 is the volume of tubing from the regulator outlet to the pressure transducer. Using Eq. (15), the temperature at a thermocouple at the regulator outlet is calculated directly from the regulator inlet conditions, and then compared to the actual thermocouple data for model validation. The temperature increase inside the regulator due to Joule–Thomson effect is not considered for two reasons. First, data inside the regulator is unavailable for model validation. The regulator outlet temperature is what can be validated and is of interest. The temperature inside the regulator, if one needs to know, should be very close to the regulator outlet temperature given the short distance. Second, the influence from neglecting the temperature increase inside the regulator to the pressure prediction is negligible. As mentioned, the ideal-gas based pressure prediction has been able to match the data quite well despite that the associated temperature may have been underestimated with an ideal-gas approach due to Joule–Thomson effect.

Eq. (15) captures the temperature response from the pressure drop and Joule–Thomson effect. There are other physical processes such as conductive and radiative heat transfer that may contribute to the temperature data from the thermocouple. The model validation attempts have found that such heat transfer is particularly needed for matching the data when the flow rate is close to zero. In that condition, the temperature of the stagnant gas can still change due to the heat transfer with the regulator components and the environment, which is not yet modeled in previous equations. Rather than using conductive and radiative heat transfer equations which may involve additional model parameters and high computational expense, an empirical heat loss term is added to the control volume equation for the volume from the transducer to the thermocouple:

$$\frac{dT_{th}}{dt} = \frac{c_p R T_{th}}{C_v P_{tr} V} m_{tr} (T_{tr} - T_{th}) - k (T_{th} - T_{amb}) \quad (16)$$

where T_{th} represents the temperature at thermocouple, and T_{amb} is the nominal ambient temperature. With a first-order lumped heat transfer coefficient k , the heat loss due to

Table 1 – Summary of model parameters.

Parameter	Value with unit	Note
V_H	$2.6 \times 10^{-7} \text{ m}^3$	High-pressure volume
V_L	$2 \times 10^{-6} \text{ m}^3$	Low-pressure volume
V_{tr}	$1 \times 10^{-5} \text{ m}^3$	Volume from regulator outlet to pressure transducer
f	1100 N s/m	Friction coefficient
k	49200, 5000 N/s	Spring constant for each spring
F_s	548 N	Preloading
M	4.6 g	Piston mass
$S_0(x)$		From design, orifice size as a function of piston position
C_{dis}		Discharge coefficient for orifice flow, a tuned parameter
γ	1.41	Specific heat ratio for H_2
R	$4155 \text{ m}^3 \text{ Pa}/(\text{K} \cdot \text{kg})$	Gas constant for H_2

multiple mechanisms could be captured. When the flow rate after the regulator (\dot{m}_{tr}) is low (close to zero), the volume from the regulator to the thermocouple becomes similar to a closed-system with heat loss only. For example, in the square wave cycling (see Model Validation section), the heat loss term will play a major role to decrease the temperature in the near-zero flow conditions. When the flow rate becomes high, the heat loss term is negligible compared with the thermal energy from the incoming gas (1st term at the RHS of Eq. (16)), meaning that

in an open system the measured temperature is primarily dependent on the condition of the gas passing through.

The model parameters are summarized in Table 1.

Model validation

In order to validate the model, hydrogen experiments with the regulator including steady hysteresis and dynamic flow

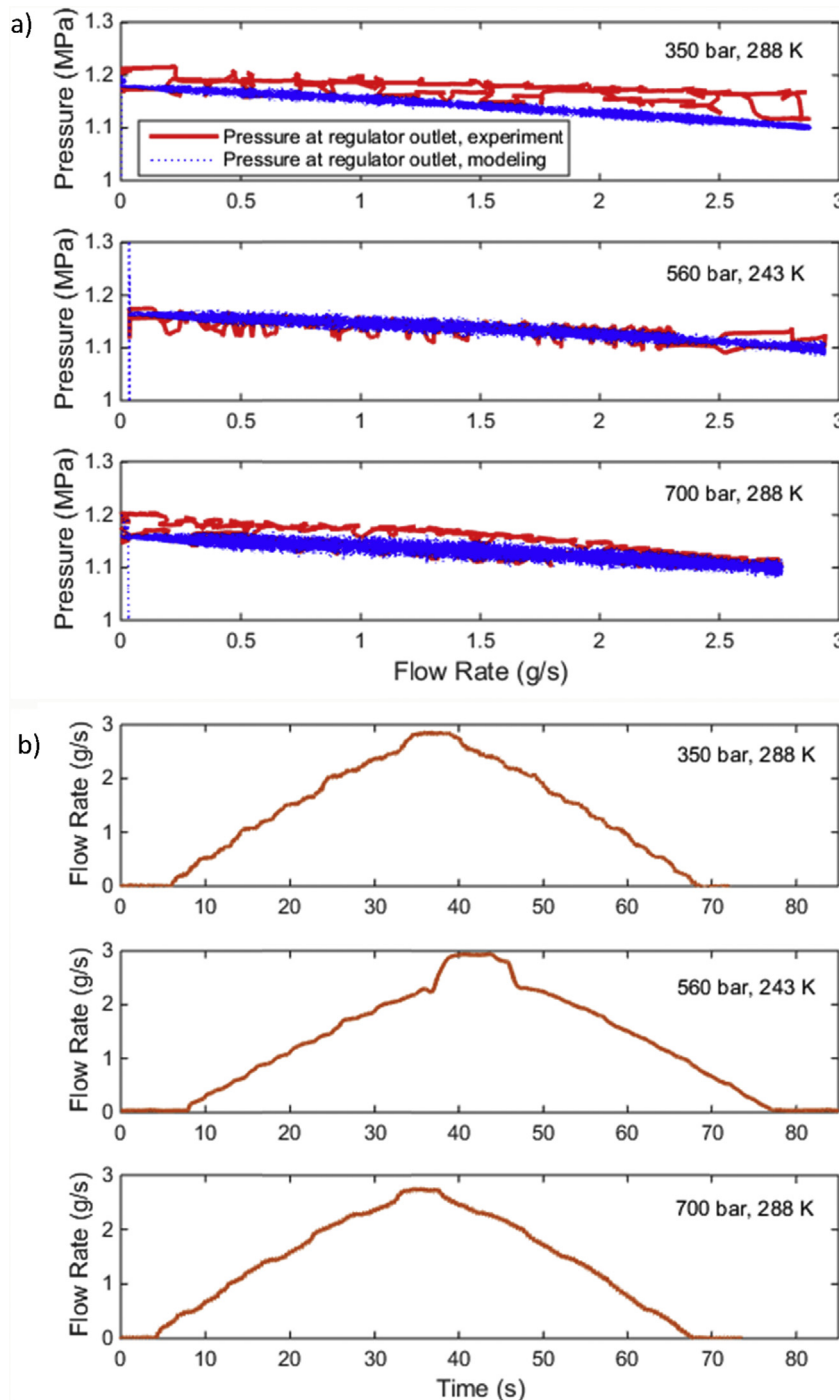


Fig. 4 – a) Experimental data and model validation of pressure at regulator outlet in three different hysteresis conditions of tank pressure and temperature. b) The flow rates with time during hysteresis tests. Note that these flow rates are from experiments and are used as model inputs as well.

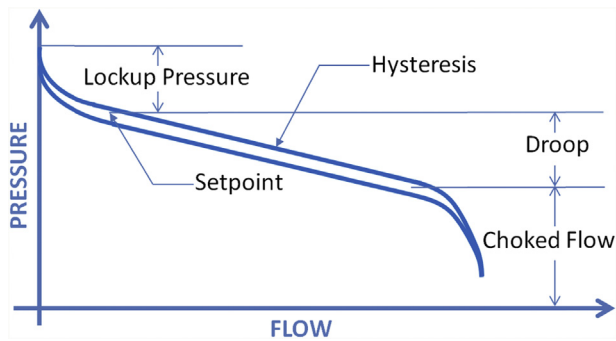


Fig. 5 – Generic example of hysteresis performance of a pressure regulator [14].

testing have been conducted. The hysteresis test involves increasing the flow rate slowly followed by symmetric decrease as shown in Fig. 4(b). The model was used to produce the same pressure response. Hysteresis associated with the change in output pressure due to the flow increase or decrease often occurs in mechanical systems due to friction forces caused by the compression and relaxation of springs or seals, as shown in an example in Fig. 5. Typically, the regulator outlet pressure hysteresis curve will be higher with decreasing flow than with increasing flow. A narrow hysteresis is a preferred characteristic to ensure the outlet pressure remains within the specified tolerance. As shown in the example in Fig. 5, the outlet pressure will decrease with increasing flow rate until the regulator poppet is fully open and choked flow is realized, which is known as droop. The desire is to operate with a flow rate below the choked flow. As expected with flow through an orifice, the outlet pressure curve with flow will

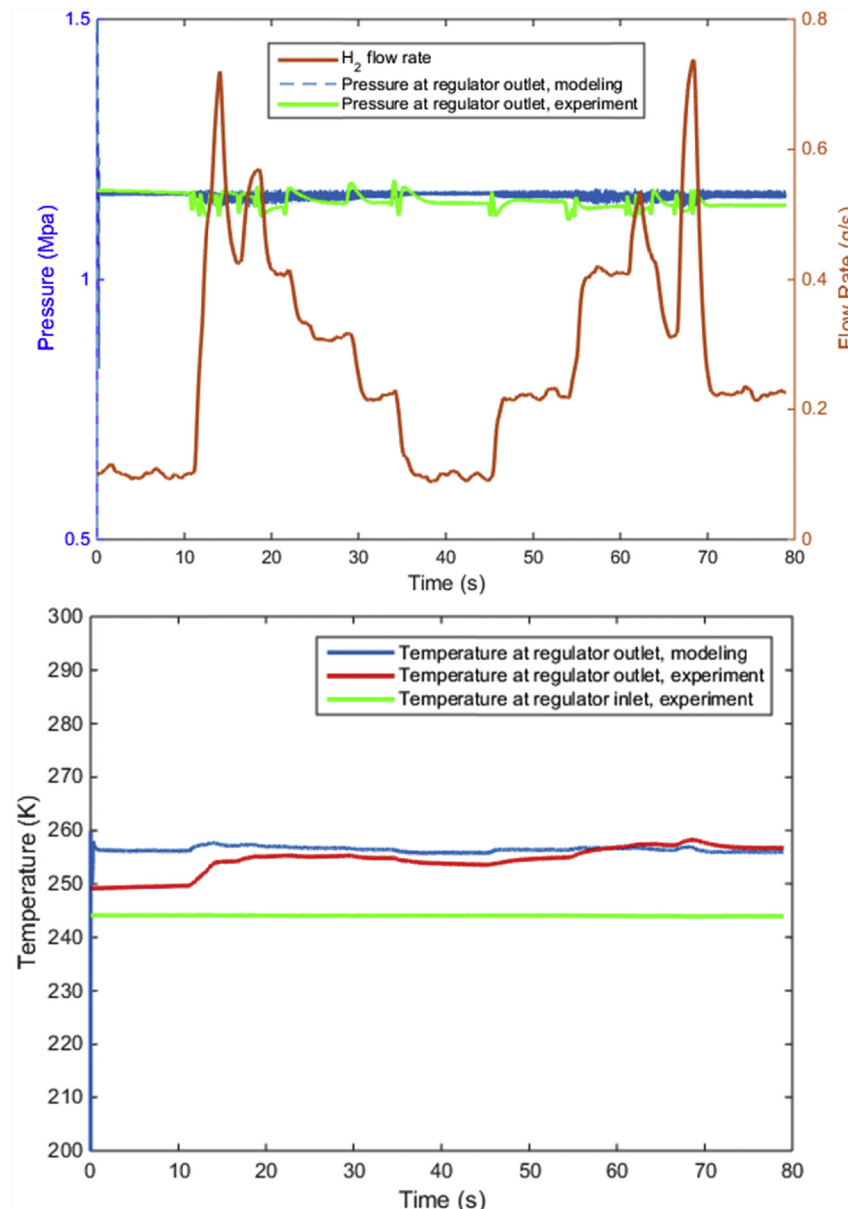


Fig. 6 – Model validation in HWY cycle with a nominal tank pressure of 550 bar and temperature of 243 K.

typically shift higher with higher inlet pressures although effective regulator designs attempt to minimize this effect. The lockup pressure is the phenomenon that occurs when the regulator poppet closes at low or no flow resulting in an uncontrollable pressure increase at the downstream. The hysteresis test is a typical way to examine the regulator performance with a steady increase in flows. The regulator used to validate the model has exhibited narrow hysteresis and small droop, therefore being accurate, for three operating conditions as shown in Fig. 4(a). The model has shown good agreement with the data in these conditions, although the outlet pressure difference with decreasing and increasing flow could not be captured by modeling because the frictions are not modeled in detail.

The hysteresis condition is akin to the steady-state operation as the flow is changing relatively slowly. To be rigorous,

additional model validation has been performed with four dynamic flow cycles based on EPA drive cycles and other operating modes: HWY cycle, FUDS cycle, startup cycle and square cycle, where the flow is changing rapidly. For HWY, FUDS and startup cycles, two operating conditions are validated; for startup cycle one operating condition is validated. Operating condition refers to a nominal tank pressure and environmental temperature when collecting the data at the test bench. The nominal pressures and temperatures for the operating conditions are noted in the figure captions as a starting reference although the actual tank pressure and temperature slowly decrease during the testing due to the hydrogen discharge. The actual time-dependent regulator inlet pressure and temperature data from experiments, rather than these nominal values, are used as model inputs, along with the flow rate requirement. The model then calculates the

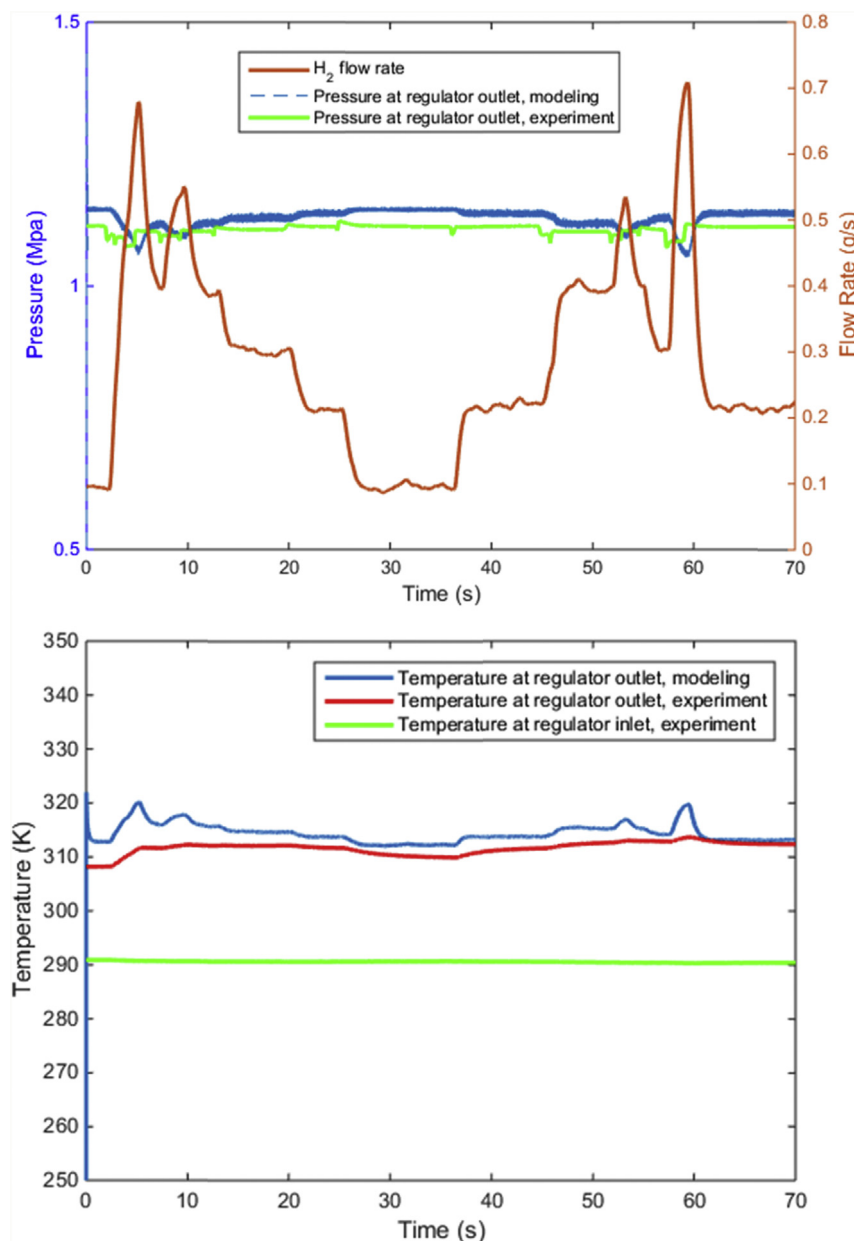


Fig. 7 – Model validation in HWY cycle with a nominal tank pressure of 610 bar and temperature of 291 K.

regulator outlet pressure and temperature responses which are compared with the data. Figs. 6–12 show the validation results in these cases. On the top of these figures, the pressure responses are plotted from both modeling and experiment, the flow rate as model input is co-plotted. On the bottom, the modeled and measured temperature responses at the regulator outlet are presented, along with the regulator inlet temperature as a reference.

In all cases, the model validation with experimental data has shown satisfactory agreement as summarized in Table 2. The averaged errors in degree and in percentage between modeling and experimental data are calculated within the selected period covering at least two cycles. A maximum average error of 2.7° (or 0.87% average percentage error referenced to the measured temperature) is found in HWY

cycles, and only $\sim 0.5^\circ$ averaged error is observed in start-up and square-wave cycles. More importantly, the modeled regulator outlet pressure and temperature both can capture the evolution trends of the data. For example, in the FUDS case (Fig. 9) the modeled pressure closely tracked the pattern of data with time even though there has been a small over-prediction. The modeled temperature is also consistent with data in every temperature increase or decrease, and the small over-prediction converges after 40 s. Finally, the model has been able to capture peak temperatures in all cases, despite a small over-prediction in some cases which may be necessary as a safety margin. With the comprehensive validation, the model is now ready for use in supporting further design evaluations and parametric studies of optimal operation to remain within the pressure and temperature limits.

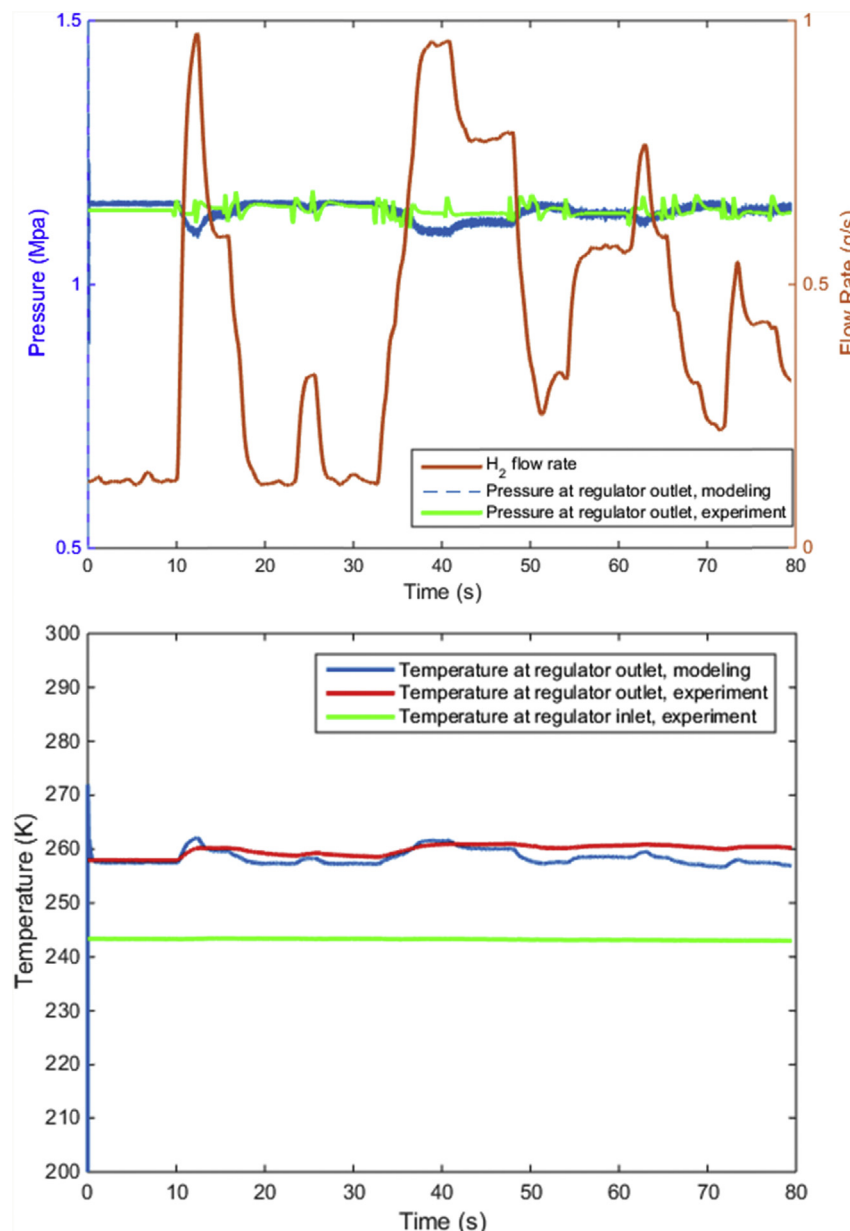


Fig. 8 – Model validation in FUDS cycle with a nominal tank pressure of 550 bar and temperature of 243 K.

Parametric study

Since the model has shown success in validation, parametric studies are presented in this section to demonstrate how the model can be used to investigate the influences of operating conditions on hydrogen discharge behaviors. Given a specific regulator design, the user may not be able to modify certain regulator parameters. As an automotive OEM, however, it is possible to optimize the operating conditions for the best use of the regulator.

Fig. 13 presents the effects of flow-rate ramp-up rates with tank pressure and temperature of 640 bar and 291 K, respectively. Given the changing power requirements from fuel cell stack, it is necessary to adjust the hydrogen flow rate accordingly. With an 80 kW fuel cell stack operating at

0.76 V at its full-power and an anode stoichiometry (ϵ) of 1.1, the required maximum hydrogen flow rate can be calculated:

$$\dot{m} = \frac{P\epsilon}{VF} = \frac{80000W \times 1.1}{0.76V \times 96485C/mol} = 1.2 \frac{mol}{s} = 2.4 \frac{g}{s} \quad (17)$$

Therefore, the hydrogen flow rate is cycled between 0.1 and 2.4 g/s for two continuous cycles in the parametric studies. In the top subplot in Fig. 13, the flow rate increases with a ramp-up rate of 1 g/s, 1.92 g/s, and 4.6 g/s per second, respectively, along with holding at lower limit of 0.1 g/s and upper limit of 2.4 g/s for a few seconds. The regulator inlet pressure is 640 bar and temperature is 291 K. As shown in the middle subplot, the resulted pressures at regulator outlet are almost overlapping at ~1.11 MPa at the 2.4 g/s flow rate hold, regardless of the ramp-up rate. Therefore, the regulator with chosen design parameters is able to maintain the downstream

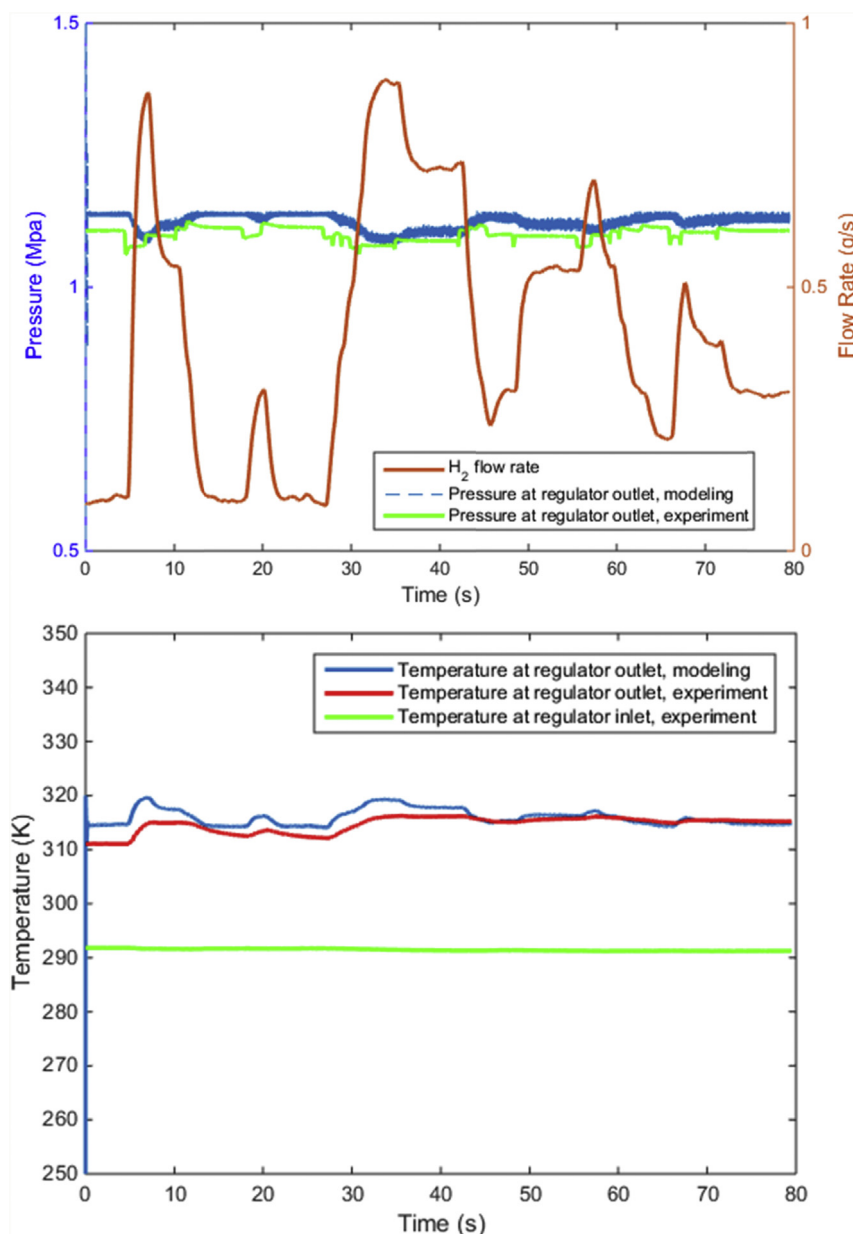


Fig. 9 – Model validation in FUDS cycle with a nominal tank pressure of 640 bar and temperature of 291 K.

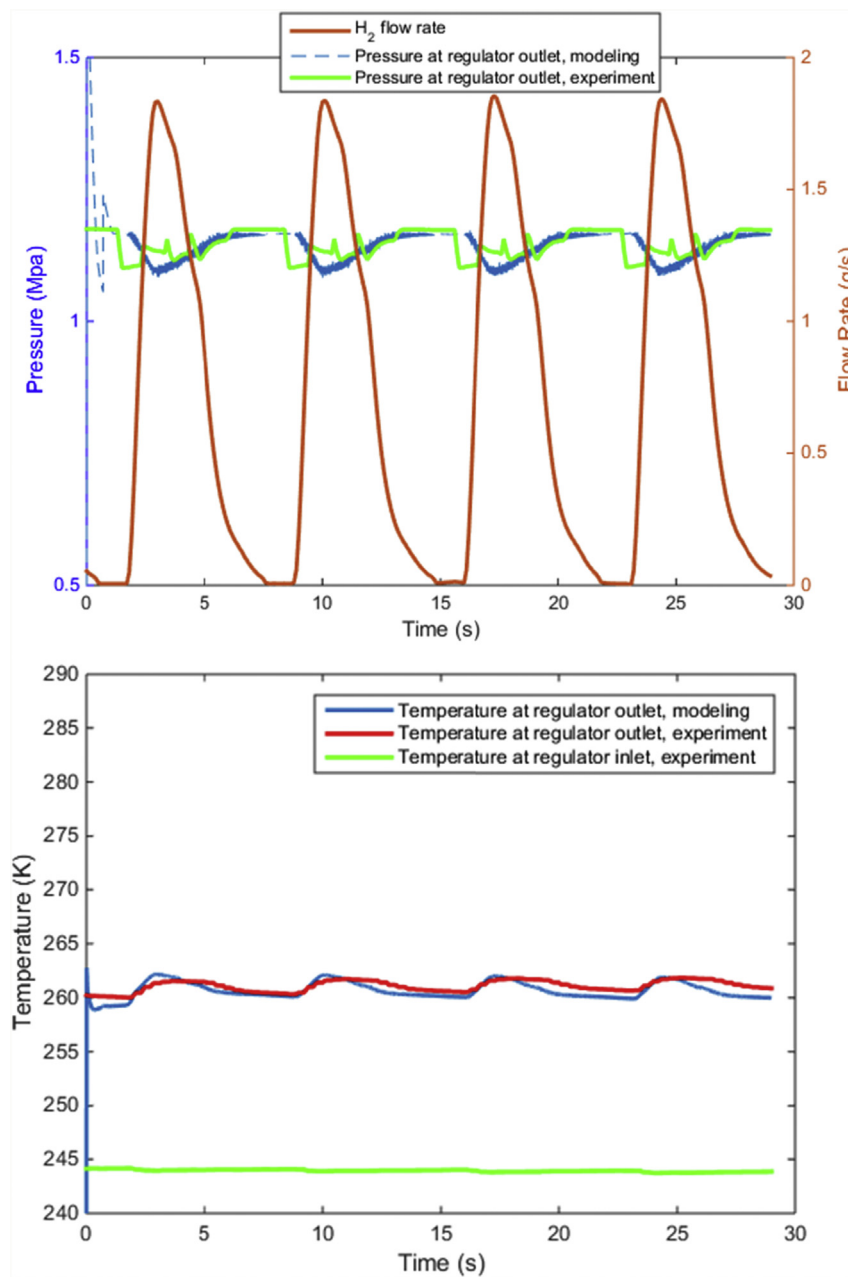


Fig. 10 – Model validation in startup cycle with a nominal tank pressure of 550 bar and temperature of 243 K.

pressure even if the flow rate is increased rapidly, which is a desired feature. In the bottom subplot, the temperature at the regulator outlet exhibits similar evolution patterns to the pressure. The alignment of these results is expected since the temperature submodel is an algebraic equation involving pressure drop across the regulator. The Joule–Thomson effect can be observed as the regulator outlet temperature cycles between ~ 315 and ~ 319 K, much higher than the regulator inlet temperature of 291 K. When the flow rate is highest (2.4 g/s), the pressure drop across the regulator is greatest, thus the regulator outlet temperature (~ 319 K) also reaches the peak. In summary, changing flow-rate ramp-up rate seems to have negligible effects on the steady-state pressure and temperature at the regulator outlet.

Fig. 14 compares the effect of regulator inlet pressure on the regulator outlet pressure and temperature when the flow rate is ramping up at 1 g/s. The three inlet pressures chosen represent a wide range of practical hydrogen tank pressures. The hydrogen tank on a fuel cell vehicle typically utilizes a nominal working pressure of 700 bar for maximizing the energy density and increasing the driving range. The maximum fill pressure of the tank is 875 bar to allow for the temperature increase during fueling while maintaining density at 700 bar.

Higher regulator inlet pressure results in a higher flow rate based on Eq. (9) (flow rate depends on only P_{hi} in this case), and thus lower regulator outlet pressure as shown in the middle subplot in Fig. 14. The outlet pressures maintain consistent values within ~ 0.03 bar, which is highly desired to provide the

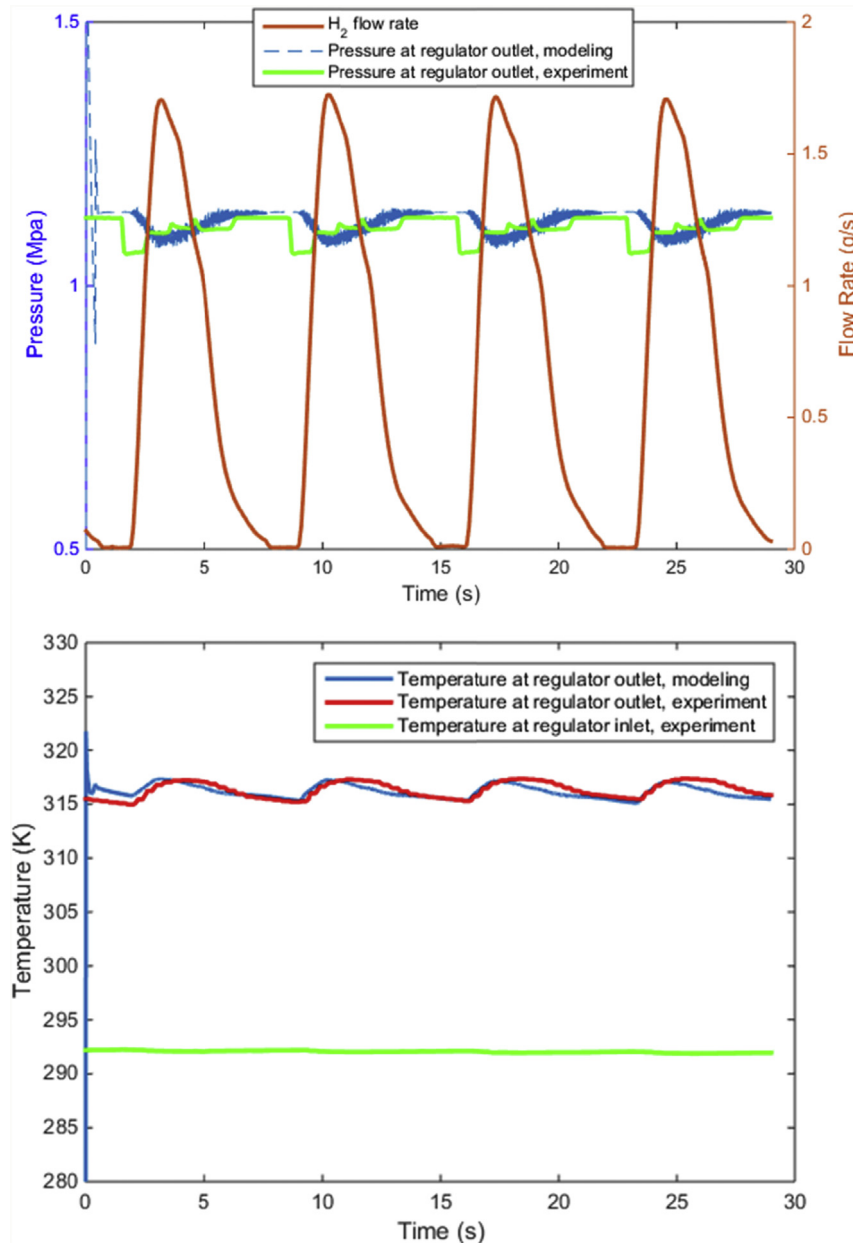


Fig. 11 – Model validation in startup cycle with a nominal tank pressure of 640 bar and temperature of 291 K.

necessary performance to the fuel cell. On the other hand, the higher inlet regulator pressure has significantly greater pressure drop and therefore greater regulator outlet temperature. As can be seen in the bottom subplot, when the regulator inlet pressure is 875 bar, the regulator outlet temperature can reach as high as ~355 K, an increase of 64 K from the regulator inlet temperature. Thus, in order to manage the fuel cell system temperature limitation of 85 °C, the vehicle design should ensure the regulator is not directly coupled with the fuel cell stack; rather the regulator should be sufficiently spaced to allow heat dissipation with the interconnected tubing.

The effect of regulator inlet or tank temperature has also been investigated as shown in Fig. 15. From the middle subplot, varying regulator inlet temperature and maintaining the same regulator inlet pressure does not seem to have an effect

on the regulated pressure. On the other hand, the bottom subplot illustrates a higher regulator outlet temperature corresponding to a higher regulator inlet temperature. A 125° difference in regulator inlet temperature from 233 to 358 K has led to approximately 140° difference at the regulator outlet from 269 K to 409 K at 2.4 g/s flow rate. Nevertheless, alleviating the temperature spike due to Joule–Thomson effect by reducing the hydrogen tank temperature may not be an effective approach given the parasitic power for cooling.

Table 3 provides a summary of the parametric study, showing the relative impacts of three controllable operating parameters on the regulator output performance. For comparison purpose, the parametric sensitivity is quantified as the ratio of the percentage change in the output versus the percentage change in the control factor. For example, when

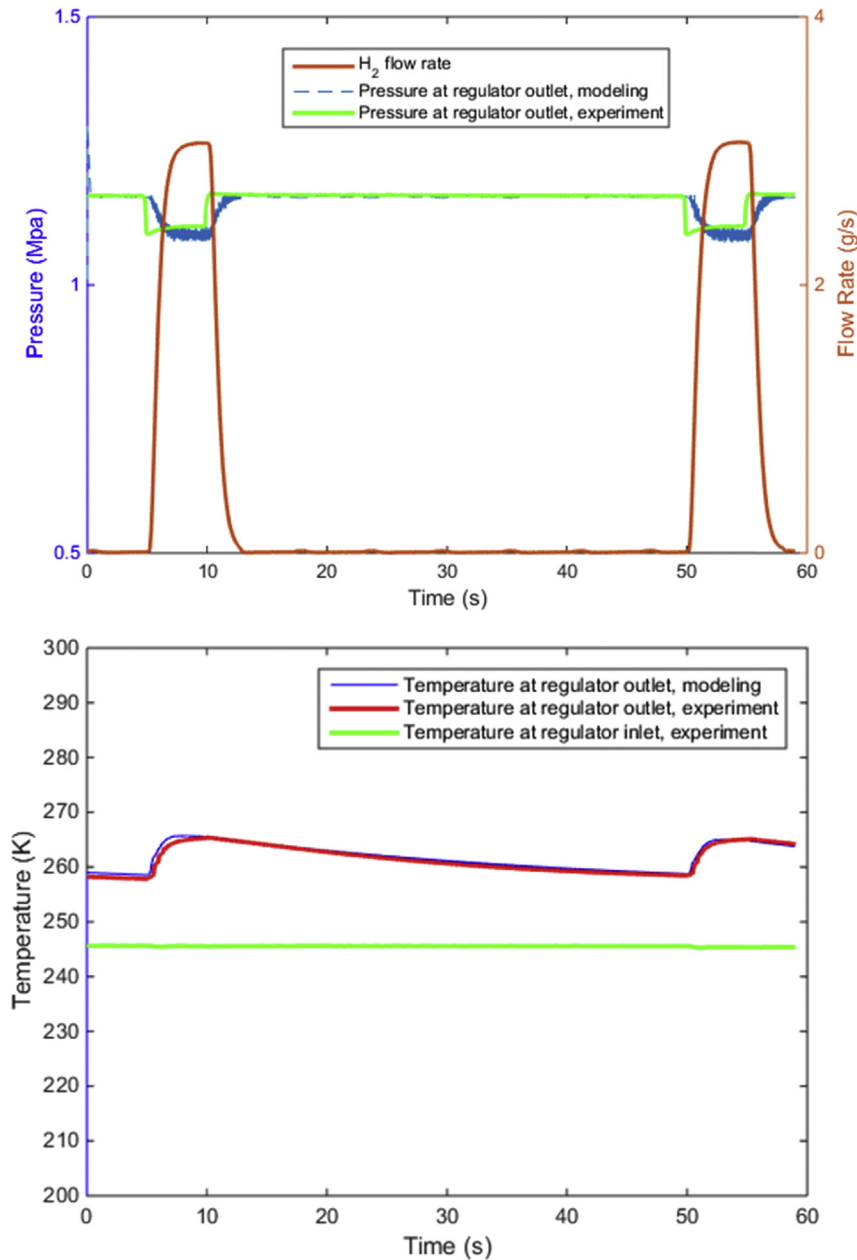


Fig. 12 – Model validation in square cycle with a nominal tank pressure of 600 bar and temperature of 243 K.

Table 2 – Comparison of modeling and experimental data.

		Average Error (degree)	Average Percentage Error	Trend Captured?	Peak Temperature
Start-up	550 bar 243 K	0.55	0.21%	Yes	Captured
	640 bar 291 K	0.45	0.14%	Yes	Captured
HWY	550 bar 243 K	2.4	0.94%	Yes	Captured
	610 bar 291 K	2.7	0.87%	Yes	Over ~6 K
FUDS	550 bar 243 K	1.6	0.62%	Yes	Captured
	640 bar 291 K	1.5	0.48%	Yes	Over ~3 K
Square	600 bar 243 K	0.47	0.18%	Yes	Captured

regulator inlet pressure increases from 500 bar to 875 bar or increases 75%, the outlet temperature has shown a response from ~301 K to ~355 K at steady state which is a 17.9% increase. Thus, the sensitivity of outlet steady-state temperature to

inlet pressure is $17.9\%/75\% = 0.24$. A greater number in absolute value in Table 3 represents a higher sensitivity, and a negative number indicates a reduced output when increasing a control factor.

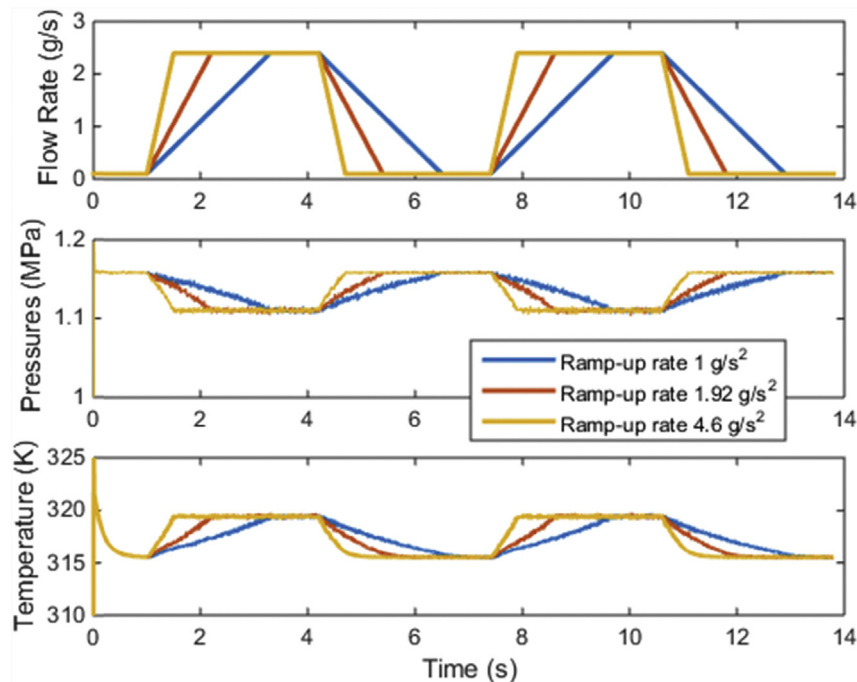


Fig. 13 – The influence of flow rate ramp-up rate (1 g/s, 1.92 g/s, and 4.6 g/s) on regulator outlet pressure and temperature. The regulator inlet pressure and temperature are 640 bar and 291 K, respectively.

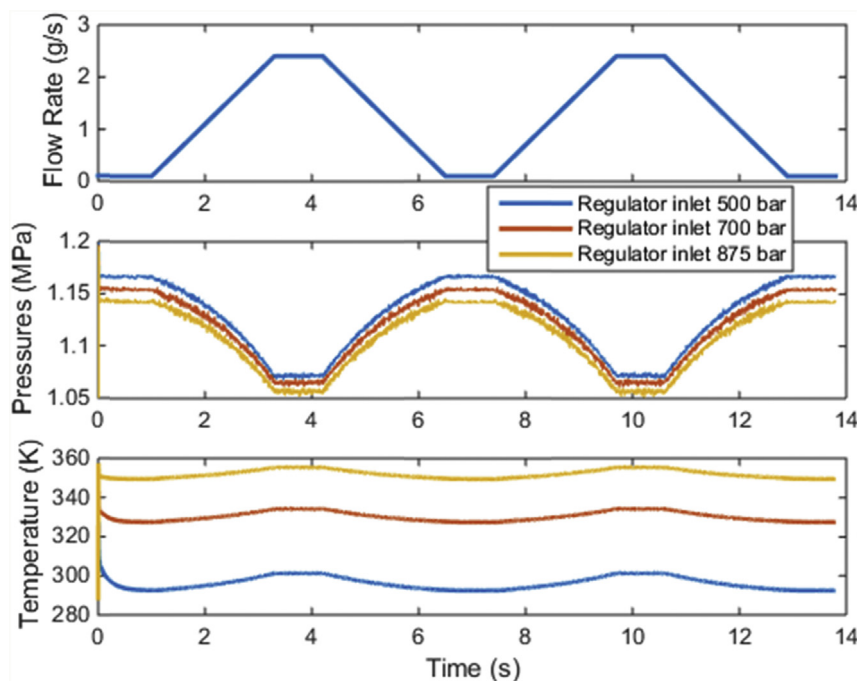


Fig. 14 – The influence of regulator inlet pressure on regulator outlet pressure and temperature. The flow-rate ramp-up rate is 1 g/s and the regulator inlet temperature is 291 K.

As can be seen in Fig. 13, flow rate ramp-up rate directly determines the temporal evolution patterns for regulator outlet pressure and temperature, but seems to have negligible influence on the steady-state outputs. Changing regulator inlet pressure and temperature, as a contrast, affects the

steady-state outlet pressure and temperature effectively but not the transients. These negligible sensitivities are also reported in Table 3. One should note that this modeling work has focused on the temperature and pressure of the gas passing through the regulator. The regulator components are

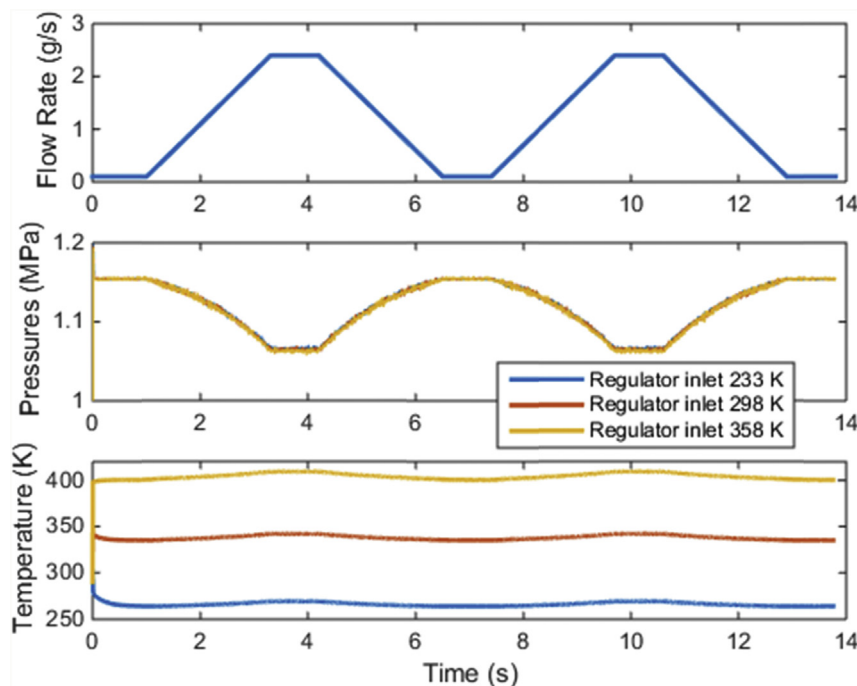


Fig. 15 – The influence of regulator inlet temperature on regulator outlet pressure and temperature. The flow-rate ramp-up rate is 1 g/s and the regulator inlet pressure is 640 bar.

Table 3 – Summary of parametric sensitivities quantified as the ratio of the percentage change in output versus the percentage change in control factor.

Regulator outputs Control factors	Outlet pressure		Outlet temperature	
	Steady-State	Transients	Steady-State	Transients
Flow rate ramp-up rate	Negligible	1	Negligible	1
Inlet pressure	-0.02	Negligible	0.24	Negligible
Inlet temperature	Negligible	Negligible	0.97	Negligible

not considered in modeling. These components may exhibit different transient and steady-state temperatures from the gas depending on their thermal mass as well as heat transfer with gas, although the impact from gas temperature is certainly significant. The steady-state regulator outlet pressure shows variation in Figs. 14 and 15 in responding to the inlet pressure and temperature changes, which can confirm the effectiveness of regulator design. The inlet temperature exhibits stronger effect on the steady-state outlet temperature than the inlet pressure does. Nevertheless, controlling inlet pressure would be more feasible to implement to avoid overheating at outlet due to Joule–Thomson effect, given that reducing inlet temperature may need parasitic power for cooling and longer time.

Conclusion

In this work, a pressure regulator model with the consideration of Joule–Thomson effect for hydrogen has been developed. The model has been able to capture both the pressure response and the temperature increase associated

with the pressure reduction during hydrogen delivery, as validated with data from various dynamic flow conditions. A constant-enthalpy through the regulator was used to derive the temperature at the regulator outlet, which is mathematically convenient rather than the non-ideal gas approaches [19,20] in capturing the Joule–Thomson effect. To the best of the authors' knowledge, the regulator model is the first comprehensive model in the literature that has captured the Joule–Thomson effect for hydrogen and pressure prediction along with experimental validations. The validated model can be used to study operating and design factors. For example, the parametric study has shown that the flow ramp-up rate has a negligible effect on the steady-state pressure and temperature, whereas changing the regulator inlet pressure and temperature can effectively influence the steady-state temperature at regulator outlet. Although the steady-state outlet temperature seems to have a relatively high sensitivity to inlet temperature, it may be more feasible to restrict inlet pressure in avoiding overheating at outlet due to Joule–Thomson effect. This regulator model can also be integrated into a complete fuel cell system and vehicle model (for example, Ref. [28]) to study

other operational characteristics particularly those pertaining temperature limitations.

Nomenclature

A	Surface area in contact with hydrogen, m ²
E	Internal Energy, J
F _s	Pre-loaded spring force, N
M	Mass of piston, kg; or molar mass, g/mol
P	Pressure, Pa
R	Gas constant
S ₀	Orifice size, m ²
T	Temperature, K
V	Volume, m ³
Z	Compressibility factor
c	Discharge coefficient
c _p	Specific heat at constant pressure, J/K
c _v	Specific heat at constant volume, J/K
f	Friction coefficient, (N s)/m
h	Enthalpy, J
k	Spring constant N/m
m	Mass, kg
x	Location of piston, m
γ	Specific heat ratio (c _p /c _v)
ρ	Density, kg/m ³
Subscript	
CV	Control volume
H/hi	High-pressure volume of regulator
L/lo	Low-pressure volume of regulator
tr	Pressure transducer downstream of regulator

REFERENCES

- [1] NREL Fuel Cell Electric Vehicle Evaluations, Available from: <https://www.nrel.gov/hydrogen/fuel-cell-vehicle-evaluation.html>.
- [2] Bao C, Ouyang M, Yi B. Modeling and control of air stream and hydrogen flow with recirculation in a PEM fuel cell system—I. Control-oriented modeling. *Int J Hydrogen Energy* 2006;31:1879–96.
- [3] Bao C, Ouyang M, Yi B. Modeling and control of air stream and hydrogen flow with recirculation in a PEM fuel cell system—II. Linear and adaptive nonlinear control. *Int J Hydrogen Energy* 2006;31:1897–913.
- [4] Hatti M, Tioursi M. Dynamic neural network controller model of PEM fuel cell system. *Int J Hydrogen Energy* 2009;34:5015–21.
- [5] Dadvar M, Afshari E. Analysis of design parameters in anodic recirculation system based on ejector technology for PEM fuel cells: a new approach in designing. *Int J Hydrogen Energy* 2014;39:12061–73.
- [6] Hong L, Chen J, Liu Z, Huang L, Wu Z. A nonlinear control strategy for fuel delivery in PEM fuel cells considering nitrogen permeation. *Int J Hydrogen Energy* 2017;42:1565–76.
- [7] Zhu Y, Li Y. New theoretical model for convergent nozzle ejector in the proton exchange membrane fuel cell system. *J Power Sources* 2009;191:510–9.
- [8] Chen J, Hu J, Waldecker J. Model-based analysis of carbon corrosion in start-up/shutdown, fuel starvation, and voltage reversal of a polymer electrolyte fuel cell. *ECS Transactions* 2017;77:1473–83.
- [9] Yang Y, Zhang X, Guo L, Liu H. Mechanisms of voltage spikes and mitigation strategies for proton exchange membrane fuel cells with dead-ended anode under pressure swing operation. *Int J Hydrogen Energy* 2017;42:28578–87.
- [10] Chen F, Zhang M, Qian J, Chen L, Jin Z. Pressure analysis on two-step high pressure reducing system for hydrogen fuel cell electric vehicle. *Int J Hydrogen Energy* 2017;42:11541–52.
- [11] Hu Z, Yu Y, Wang G, Chen X, Chen P, Chen J, et al. Anode purge strategy optimization of the polymer electrode membrane fuel cell system under the dead-end anode operation. *J Power Sources* 2016;320:68–77.
- [12] DOE Technical Targets for Onboard Hydrogen Storage for Light-Duty Fuel Cell Vehicles, Available from: <https://www.energy.gov/eere/fuelcells/doe-technical-targets-onboard-hydrogen-storage-light-duty-vehicles>.
- [13] Ahluwalia R, Wang X. Fuel cell systems for transportation: status and trends. *J Power Sources* 2008;177:167–76.
- [14] The Basics of Pressure Regulators, Available from: <http://www.beswick.com/basics-pressure-regulators>.
- [15] Nabi A, Wacholder E, Dayan J. Dynamic model for a dome-loaded pressure regulator. *J Dyn Syst Meas Contr* 2000;122:290–7.
- [16] Rami E, Jean-Jacques B, Bruno D, Francois M. Modelling of a pressure regulator. *Int J Pres Ves Pip* 2007;84:234–43.
- [17] Zafer N, Luecke G. Stability of gas pressure regulators. *Appl Math Model* 2008;32:61–82.
- [18] Sun B, Xu Q, Chen Y. Dynamic modeling and simulation of a pressurized system used in flight vehicle. *Chin J Aeronaut* 2018;31:1232–48.
- [19] Yang J. A thermodynamic analysis of refueling of a hydrogen tank. *Int J Hydrogen Energy* 2009;34:6712–21.
- [20] Ruffio E, Saury D, Petit D. Thermodynamic analysis of hydrogen tank filling Effects of heat losses and filling rate optimization. *Int J Hydrogen Energy* 2014;39:12701–14.
- [21] Dicken C, Mérida W. Measured effects of filling time and initial mass on the temperature distribution within a hydrogen cylinder during refuelling. *J Power Sources* 2007;165:324–36.
- [22] Suryan A, Kim H, Setoguchi T. Three dimensional numerical computations on the fast filling of a hydrogen tank under different conditions. *Int J Hydrogen Energy* 2012;37:7600–11.
- [23] Olmos F, Manousiouthakis V. Hydrogen car fill-up process modeling and simulation. *Int J Hydrogen Energy* 2013;38:3401–18.
- [24] Striednig M, Brandstätter S, Sartory M, Klell M. Thermodynamic real gas analysis of a tank filling process. *Int J Hydrogen Energy* 2014;39:8495–509.
- [25] de Miguel N, Acosta B, Baraldi D, Melideo R, Cebolla R, Moretto P. The role of initial tank temperature on refuelling of on-board hydrogen tanks. *Int J Hydrogen Energy* 2016;41:8606–15.
- [26] Elgowainy A, Reddi K, Lee D-Y, Rustagi N, Gupta E. Techno-economic and thermodynamic analysis of pre-cooling systems at gaseous hydrogen refueling stations. *Int J Hydrogen Energy* 2017;42:29067–79.
- [27] Lemmon E, Huber M, Leachman J. Revised standardized equation for hydrogen gas densities for fuel consumption applications. *J Res NIST* 2018;113:341–50.
- [28] Fang C, Li J, Xu L, Ouyang M, Hu J, Cheng S. Model-based fuel pressure regulation algorithm for a hydrogen-injected PEM fuel cell engine. *Int J Hydrogen Energy* 2015;40:14942–51.